

CONTENTS

	Page
ACKNOWLEDGEMENT	iii
ABSTRACT (ENGLISH)	iv
ABSTRACT (THAI)	vii
LIST OF TABLES	xiv
LIST OF FIGURES	xv
ABBREVIATIONS AND SYMBOLS	xx
CHAPTER 1 INTRODUCTION	1
1.1 Bone is a nanocomposite	1
1.2 Mechanical properties of bone	5
1.3 The present—current status of bone grafting	8
1.4 Bone graft materials	9
1.5 Hydroxyapatite (HA)	13
1.6 Nanocrystalline materials	16
1.6.1 Reduced sintering temperature	19
1.6.2 Hardness and fracture toughness	20
1.6.3 Superplasticity	22
1.7 Processing of nanocrystalline hydroxyapatite ceramics	23
1.7.1 Densification characteristics of nanocrystalline powders	24
1.7.1.1 Minimizing grain growth and maximizing densification during sintering of ultrafine particles	25

1.7.1.2 The sintering of nanopowders (nanosintering)	26
CHAPTER 2 PURPOSES OF THE RESEARCH	33
CHAPTER 3 EXPERIMENTAL PROCEDURE	37
3.1 Synthesis of nanocrystalline hydroxyapatite powder	37
3.2. Synthesis of SiO₂ nanopowder from rice husk ash	40
3.3 Experimental procedure	40
3.3.1 Thermally stability of nanocrystalline hydroxyapatite powder	40
3.3.2 Sintering of HA nanopowders with conventional sintering	41
3.3.3 Sintering of HA nanopowders with rate-controlled sintering	41
3.3.4 Fabrication of craniotomy flap fixation plates	42
3.3.5 Fabrication of Nanoporous HA ceramics	44
3.4 Structural characterization	44
3.5 Physical characterization	45
3.5. 1 Density and porosity	45
3.6 Mechanical characterization	
3.6.1 Hardness	46
3.6.2 Bending strength	46
3.6.3 Fracture toughness	47

CHAPTER 4**SYNTHESIS AND CHARACTERIZATION OF NANOCRYSTALLINE****HYDROXYAPATITE FROM NATURAL BOVINE BONE 49****4.1 Introduction 49****4.2 Experimental procedures 51****4.3 Results and Discussions 52****4.4 Conclusions 58****CHAPTER 5****SYNTHESIS OF SiO₂ NANOPOWDER FROM RICE HUSK ASH 59****5.1 Introduction 59****5.2 Experimental procedures 60****5.3 Results and Discussions 60****5.4 Conclusions 63****CHAPTER 6****THERMAL STABILITY OF NANOCRYSTALLINE HYDROXYAPATITE****POWDER 65****6.1 Introduction 65****6.2 Experimental procedures 66****6.3 Results and Discussions 67****6.4 Conclusions 72**

CHAPTER 7	
PROCESSING OF HYDROXYAPATITE NANOCERAMIC BY	
CONVENTIONAL SINTERING	74
7.1 Introduction	74
7.2 Materials and Methods	76
7.3 Results and Discussions	77
7.4 Conclusions	85
CHAPTER 8	
ENHANCEMENT OF MECHANICAL PROPERTIES OF	
NANOCRYSTALLINE HYDROXYAPATITE CERAMICS BY RATE-	
CONTROLLED SINTERING METHOD	86
8.1 Introduction	86
8.2 Experimental procedures	88
8.3 Results and Discussions	91
8.4 Conclusions	102
CHAPTER 9	
FABRICATION OF DENSE NANOCRYSTALLINE HYDROXYAPATITE	
CERAMICS FOR CRANIOTOMY FLAP FIXATION	103
9.1 Introduction	103
9.2 Experimental procedures	105
9.3 Results and Discussions	106
9.4 Conclusions	110

CHAPTER 10	
THE FABRICATION OF NANOPOROUS HYDROXYAPATITE	
CERAMICS	111
10.1 Introduction	111
10.2 Materials and methods	112
10.3 Results and Discussions	113
10.4 Conclusions	116
CHAPTER 11	
CONCLUSIONS AND FUTURE WORKS	117
11.1 Conclusions	117
11.2 Future work	118
REFERENCES	119
VITA	

LIST OF TABLES

Table		Page
1.1	Biomechanical properties of bone	8
1.2	Mechanical properties of metals	10
1.3	Mechanical properties of ceramics	10
1.4	Mechanical properties of polymers	11
1.5	Methods involved in the synthesis of HA nanopowders	23
5.1	Chemical composition and the trace elements of SiO ₂ nanopowder after heat treated at 1000°C for 3 h.	63

LIST OF FIGURES

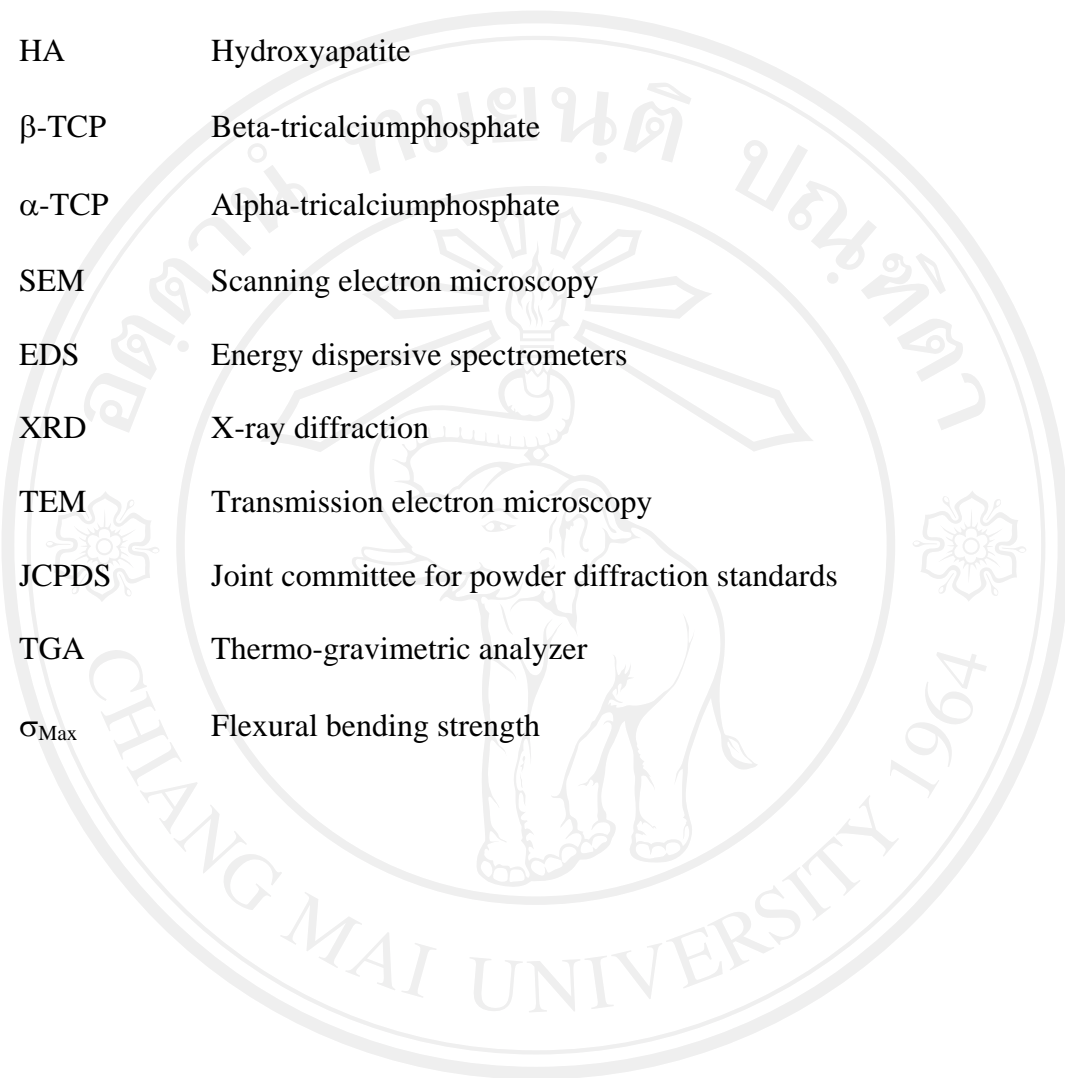
Figure	Page
1.1 The hierarchical levels of structure found in osteonal bone, as demonstrated by Weiner and Wagner	3
1.2 Hierarchical levels of structural organization in a human long bone	4
1.3 (a) Optical micrograph of transverse cross section showing the microstructure of compact lamellar bone–human femora (b) Scanning electron micrograph of plate-like cancellous bone with columnar structure	5
1.4 A representative load-deflection curve for human compact bone	6
1.5 SEM of as-fractured bone	7
1.6 Prototypes of HA-based bone graft materials. (a) Different shapes and sizes of HA. (b) HA-coated bioimplants	13
1.7 Two-dimensional model of a nanostructured material. The atoms in the centers of the crystals are indicated in black. The ones in the boundary core regions are represented as open circles	18
1.8 The effect of grain size on calculated volume fractions of intercrystal regions and triple junctions, assuming a grain-boundary thickness of 1 nm	18
1.9 Reduction in sintering temperature through the use of nanocrystalline grain sizes. “G” values indicate green densities	20
1.10 Hardness as a function of density for nanocrystalline and submicron-grained zirconias	21

Figure	Page
1.11 Schematic diagram of an agglomerated powder	25
1.12 Different stages in densification of compacts	27
1.13 SEM micrograph of the resulting bioceramic sintered 1200°C for 3 h	30
1.14 SEM micrograph of the fracture surface for samples sintered at 1200°C	31
3.1 A diagram of preparation of nanocrystalline hydroxyapatite powder	39
3.2 Difference two sintering methods (a) linear heating rate sintering and (b) non-linear heating rate sintering.	43
3.3 The ball-on-ring tests	47
3.4 Cracking around hardness indentation	48
4.1 X-ray diffraction patterns of HA powders at various vibro-milling times compared with JCPDS file 9-432 of pure HA.	53
4.2 The linear regression of $B_{\text{crystalline}}$ versus vibro-milling time using the same reflection of (202) plane from the XRD pattern of each HA powder.	54
4.3 SEM micrographs of HA powders at various vibro-milling time, (a) 2h (b) 8h.	55
4.4 EDS spectrum of nanocrystalline HA powders and the result of the chemical analysis determined by EDS technique (inset).	57
4.5 TEM micrographs of nanocrystalline HA powders and corresponding diffraction ring pattern (inset).	58
4.6 TEM images of two lattice fringes of (a) (100) and (b) (101) planes.	59
5.1 XRD of RHA after 4 h vibro milling time and after heat treatments at 1000°C.	61

Figure	Page
5.2 SEM micrographs of the RHA sample: (a) after 4 h vibro milling time and (b) after heat treatments at 1000°C.	62
5.3 (a) rice husk ash (b) After 4 h vibro-milling time and (c) After burning out at 1000°C for 3 h.	64
6.1 SEM micrographs of HA nanoneedle-like structure.	68
6.2 XRD pattern of HA nanoneedle-like structure compared with JCPDS file 9-432 of pure HA.	69
6.3 X-ray diffraction patterns of nanocrystalline HA powders after heated at 1000°C, 1100°C, 1150°C:(c), 1200°C, 1250°C and 1300°C compared with JCPDS file 9-432 of pure HA.	70
6.4 TGA result of HA nanopowder.	71
6.5 SEM micrographs of nanocrystalline HA powders after heated at 1000°C:(a), 1100°C:(b), 1150°C:(c), 1200°C:(d) 1250°C:(e) and 1300°C:(f).	73
7.1 X-ray diffraction patterns of various HA ceramics sintered at 1200°C for vibro-milling times (0-8h).	77
7.2 X-ray diffraction patterns of various HA ceramics sintered at 1300°C for vibro-milling times (0-8h).	78
7.3 Density as a function vibro-milling time for the HA ceramics sintered at 1200 and 1300°C.	79
7.4 Fracture surfaces of various HA ceramics sintered at 1200°C for various vibro-milling time; (a) 0 h, (b) 1 h, (c) 2 h, (d) 4 h, and (e) 8 h.	81

Figure	Page
7.5 Fracture surfaces of HA ceramics sintered at 1200°C for the vibro-milling times of: (a) 2 h and (b) 4 h. Arrows indicate the nanostructure HA grains embedded in the micron sized grains.	81
7.6 Fracture surfaces of HA ceramic sintered at 1300°C; (a) 0 h, and (b) 8h.	82
7.7 Effect of vibro-milling time on Vickers microhardness of the HA ceramics sintered at 1200 and 1300°C.	83
7.8 Effect of vibro-milling time on flexural bending strength of the HA ceramics sintered at 1200 and 1300°C.	84
8.1 Sintering programs for:(a) conventional method and (b) rate-controlled sintering method.	90
8.2 SEM micrographs of HA powders: (a) after vibro-milling, (b) after ultrasonic treatment.	91
8.3 XRD pattern of HA nanopowder.	92
8.4 XRD for HA ceramics: (a) conventional sintering method, (b) rate-controlled sintering	94
8.5 Density of HA ceramics prepared by normal sintering and rate-controlled sintering method.	96
8.6 Fracture surfaces of HA ceramics prepared by normal sintering method (a-d) and rate control sintering methods (e-h) sintered at:1150°C (a and e), 1200 °C (b and f), 1200 °C (c and g), and 1250 °C (d and h).	98
8.7 Nanowire structure at the fracture surface of HA ceramics prepared by rate control sintering methods.	99

Figure	Page
8.8 Vickers hardness as a function of sintering temperature of HA ceramics prepared by normal sintering method and rate control sintering methods.	100
8.9 Bending strength as a function of sintering temperature of HA ceramics prepared by normal sintering method and rate control sintering methods.	102
9.1 Sintering program.	106
9.2 SEM micrographs of nanoneedle-like structure of HA.	107
9.3 XRD pattern of HA nanoneedle-like structure compared with JCPDS file 9-432 of pure HA.	107
9.4 Representative Vickers indentation obtained on the surface of sintered samples at 1200°C for 3 h.	108
9.5 SEM micrographs of fracture surface of samples: (a) low magnification and (b) high magnification.	109
9.6 Dense HA button, made from HA nanopowders (the scale shows centimeters).	110
10.1 XRD patterns of sintered samples at 1200°C.	113
10.2 SEM micrograph of HA-PVA nanocomposite powder.	114
10.3 SEM micrograph of fracture surface of nanoporous HA ceramics: (a) low magnification and (b) high magnification.	115

ABBREVIATIONS AND SYMBOLS

HA	Hydroxyapatite
β -TCP	Beta-tricalciumphosphate
α -TCP	Alpha-tricalciumphosphate
SEM	Scanning electron microscopy
EDS	Energy dispersive spectrometers
XRD	X-ray diffraction
TEM	Transmission electron microscopy
JCPDS	Joint committee for powder diffraction standards
TGA	Thermo-gravimetric analyzer
σ_{Max}	Flexural bending strength

ลิขสิทธิ์มหาวิทยาลัยเชียงใหม่
Copyright© by Chiang Mai University
All rights reserved